Shape-induced phenomena in finite-size antiferromagnets

Helen V. Gomonay and Vadim M. Loktev
Bogolyubov Institute for Theoretical Physics, NAS of Ukraine, Metrologichna street 14-b, 03680, Kyiv, Ukraine
(Received 17 February 2007; revised manuscript received 12 April 2007; published 25 May 2007)

It is common knowledge that the direction of the easy axis in a finite-size ferromagnetic sample is controlled by its shape. In the present paper we show that a similar phenomenon should be observed in compensated antiferromagnets with strong magnetoelastic coupling. The destressing energy which originates from the long-range magnetoelastic forces is analogous to the demagnetization energy in ferromagnetic materials and is responsible for the formation of the equilibrium domain structure and the anisotropy of macroscopic magnetic properties. In particular, the crystal shape may be a source of additional uniaxial magnetic anisotropy which removes the degeneracy of the antiferromagnetic vector or the artificial fourth-order anisotropy in the case of a square cross-section sample. In the special case of antiferromagnetic nanopillars, shape-induced anisotropy can be substantially enhanced due to lattice mismatch with the substrate. These effects can be detected by magnetic rotational torque and antiferromagnetic resonance measurements.

DOI: 10.1103/PhysRevB.75.174439 PACS number(s): 75.60.Ch, 46.25.Hf, 75.50.Ee

I. INTRODUCTION

The fact that antiferromagnetic crystals break up into regions with different orientations of the antiferromagnetic vectors below the Néel temperature was predicted theoretically by Néel[1] and then proved experimentally (see, e.g., Refs. 2–7 and many others).

Domain structures observed in different antiferromagnets have some common features that we summarize below.

(i) Magnetic domains with different orientations of the antiferromagnetic vector are characterized by different tensors of spontaneous strain and so can be treated as deformation twins.

(ii) The morphology of antiferromagnetic domains is similar to the morphology of deformation twins in martensites. In contrast to ferromagnets, the domain structure in antiferromagnets is regular and periodic and consists of alternating stripes with different deformation.

(iii) Unlike those of ferromagnets, domain walls separating domains with nonparallel antiferromagnetic vectors are planelike and are parallel to low-index atomic planes.

(iv) The deformation does not map the orientation of the antiferromagnetic vector locally (e.g., inside the domain wall, the orientation of the antiferromagnetic vector is determined by competition between the exchange interaction and deformation-induced anisotropy).

(v) Antiferromagnetic domains spontaneously appear below the Néel temperature. The domain patterns observed during heating-cooling cycles through the Néel point may be either identical or similar to each other.

(vi) The domain structure may be reversibly changed by external magnetic field or stress.

The properties (i)–(iv) show that magnetoelastic coupling plays the leading role in the formation of domain structure in antiferromagnets. It follows from (v) and (vi) that the domain structure may be considered as thermodynamically equilibrium, notwithstanding the fact that formation of the domain walls is associated with a positive contribution to the free energy of the whole sample. Regularity of the domain structure [properties (ii) and (iii)] excludes the entropy of domain disorder as a factor leading to a decrease of free energy of a sample and favoring formation of an inhomogeneous state.[8] The properties (iv)–(vi) may be explained by the presence of elastic defects[9] (dislocations, disclinations, etc.) that produce an inhomogeneous stress field in a sample. This "frozen-in" *extraneous* (with respect to an ideal crystal) field stabilizes the inhomogeneous distribution of antiferromagnetic vectors via magnetoelastic interactions and ensures reconstruction of the domain structure during heating-cooling cycles.

Another model[10] consistent with all the above mentioned properties is based on the assumption that antiferromagnetic ordering is accompanied by the appearance of so-called quasiplastic stresses[11] coupled with orientation of the antiferromagnetic vector. We assume that these *intrinsic* stresses are caused by virtual forces that represent the change of free energy of the system with displacement of an atom bearing a magnetic moment. The self-consistent distribution of the internal stress field depends upon the shape of the sample and is generally inhomogeneous. The equilibrium distribution of the antiferromagnetic vectors maps the stress field and thus is also inhomogeneous and sensitive to application of an external field and temperature variation.

Both the defect-based and defectless models exploiting the magnetoelastic mechanism predict similar dependence of the macroscopic characteristics of a sample vs external magnetic and stress field, but lead to different results when applied to a set of different samples. Namely, in the framework of the defect-based model, the domain distribution, domain size, and some other quantitative characteristics may vary depending on technological conditions and prehistory of a sample. On the contrary, the defectless model predicts variation of the macroscopic properties of antiferromagnetic crystals with variation of their shape.

Below we predict shape-related phenomena in antiferromagnets that can be experimentally tested. In the framework of the defectless model we calculate the effective shape-induced anisotropy, which can be determined by torque measurements, and the frequency of the lowest spin-wave branch, detectable by the antiferromagnetic resonance technique. We consider the case of an easy-plane antiferromagnet, a typical example of which is given by NiO, $CoCl_2$, or $KCoF_3$.

II. DESTRESSING ENERGY

According to our main assumption, an antiferromagnetic vector $\mathbf{L}(\mathbf{r})$ may be treated as a quasidefect that produces an intrinsic stress field $\hat{\sigma}^{(\mathrm{in})}(\mathbf{r})$. Thus, the thermodynamic potential of the finite-size antiferromagnet can be represented as (see, e.g., Ref. 10)

$$\Phi[\mathbf{L}(\mathbf{r})] = \int_V \left(f^{\mathrm{mag}}[\mathbf{L}(\mathbf{r})] - \frac{1}{2}\hat{\sigma}^{(\mathrm{in})}[\mathbf{L}(\mathbf{r})]:\hat{c}^{-1}:\hat{\sigma}^{(\mathrm{in})}[\mathbf{L}(\mathbf{r})] \right) d\mathbf{r} + \Phi^{\mathrm{dest}}. \quad (1)$$

Here f^{mag} is the "bare" magnetic energy, the second term is the self-energy of a quasidefect, $\hat{c}^{-1}$ is a fourth-rank tensor of elastic stiffness, and Φ^{dest} is the destressing energy,[10] which describes the interaction between quasidefects localized at different points. The notation is used to denote an inner product between second-rank tensors.

The explicit expression for the destressing energy is obtained from the requirement for mechanical equilibrium with due account of the boundary conditions at the sample surface. The main nonnegative contribution arises from the averaged (over the sample volume V) internal stress $\langle\hat{\sigma}^{\mathrm{in}}\rangle$ and can be represented as

$$\Phi^{\mathrm{dest}} = \frac{V}{2}\langle\sigma^{\mathrm{in}}_{jl}\rangle\aleph_{jklm}\langle\sigma^{\mathrm{in}}_{km}\rangle, \quad \aleph_{jklm} \equiv \frac{\partial^2}{\partial r_k \partial r_m}\int_V G_{jl}(\mathbf{r}-\mathbf{r}')d\mathbf{r}', \quad (2)$$

where $G_{km}(\mathbf{r}-\mathbf{r}')$ is a three-dimensional Green's function of elasticity (with zero nonsingular part) and the fourth-rank symmetrical destressing tensor $\hat{\hat{\aleph}}$ depends upon the sample shape.

The functional dependence between the intrinsic stress tensor and antiferromagnetic vector is given by a constitutive relation which should satisfy the principles of locality, material objectivity and material symmetry. The simplest form of such a relation, which assumes isotropy of magnetoelastic properties of the medium, is

$$\sigma^{\mathrm{in}}_{jk} = \frac{\lambda_v}{3}\mathbf{L}^2\delta_{jk} + \lambda'\left(L_jL_k - \frac{\mathbf{L}^2}{3}\delta_{jk}\right), \quad (3)$$

where the coefficients λ_v and λ' define the principal stresses of magnetoelastic nature.

Substituting (2) and (3) into (1), one comes to a closed expression for the thermodynamic potential, minimization of which gives the equilibrium distribution of $\mathbf{L}$ throughout the sample.

The two terms of magnetoelastic origin in (1) have one principal distinction. The structure of the local energy contribution (second term) is defined by crystal symmetry, while the structure of Φ^{dest} depends upon the sample shape. In the framework of the phenomenological approach, the local energy contributes to the effective anisotropy constant only, while the destressing energy is responsible for the domain structure formation and may be a source of artificial fourth-order anisotropy as will be shown below.

TABLE I. Shape-induced $K^{\mathrm{elas}}_{\mathrm{is}}$ and magnetic $f^{\mathrm{mag}}_{\mathrm{in\ plane}}$ anisotropy (in erg/cm^3), and critical aspect ratio for typical easy-plane antiferromagnets (details of calculation in Ref. 12).

Crystal	$K^{\mathrm{elas}}_{\mathrm{is}}$	$f^{\mathrm{mag}}_{\mathrm{in\ plane}}$	$(a/b)_{\mathrm{cr}}$
NiO	0.8×10^4	288	1.1
$CoCl_2$	5.6×10^5	$<3\times10^4$	3.4
$KCoF_3$	3×10^6	5×10^5	1.5

III. APPLICATION TO AN EASY-PLANE ANTIFERROMAGNET

To understand the role of the destressing energy in shape-induced phenomena, we consider the simplest case of an easy-plane antiferromagnet (the point symmetry group of the crystal includes third-, fourth-, or sixth-order rotations around the Z axis) cut in the form of an elliptic cylinder with a and b semiaxes (parallel to the X and Y axes, respectively) and generatrix parallel to Z. The elastic properties of the medium are supposed to be isotropic ($c_{11}-c_{12}=2c_{44}$). In this case, the nontrivial contribution to the destressing energy takes the form

$$\Phi^{\mathrm{dest}} = \frac{V}{2}[K^{\mathrm{elas}}_2(L^2_Y - L^2_X) + K^{\mathrm{elas}}_{\mathrm{is}}(\langle L^2_X - L^2_Y\rangle^2 + 4\langle L_XL_Y\rangle^2) - K^{\mathrm{elas}}_{4\mathrm{an}}(\langle L^2_X - L^2_Y\rangle^2 - 4\langle L_XL_Y\rangle^2)], \quad (4)$$

where the effective shape-induced anisotropy constants are

$$K^{\mathrm{elas}}_2 = \frac{a-b}{a+b}\frac{(\lambda')^2(2-3\nu)+\lambda_v\lambda'}{4c_{44}(1-\nu)},$$

$$K^{\mathrm{elas}}_{\mathrm{is}} = \frac{(\lambda')^2(3-4\nu)}{8c_{44}(1-\nu)}, \quad K^{\mathrm{elas}}_{4\mathrm{an}} = \left(\frac{a-b}{a+b}\right)^2\frac{(\lambda')^2}{6c_{44}(1-\nu)}, \quad (5)$$

and $\nu=c_{12}/(c_{11}+c_{12})$ is the Poisson ratio.

The magnetic energy density of such an antiferromagnet in an external magnetic field $\mathbf{H}$ (low compared with the spin-flip value) may be written as

$$f^{\mathrm{mag}} = \frac{1}{2}K^{\mathrm{mag}}_2L^2_Z + f^{\mathrm{mag}}_{\mathrm{in\ plane}} - \frac{1}{2}\chi(\mathbf{H}\times\mathbf{L})^2, \quad (6)$$

where χ is the magnetic susceptibility, the out-of-plane anisotropy constant $K^{\mathrm{mag}}_2 \gg K^{\mathrm{elas}}_2$ is large enough to keep the antiferromagnetic vector in the XY plane, and the explicit form of the in-plane magnetic anisotropy $f^{\mathrm{mag}}_{\mathrm{in\ plane}}$ is specified by the crystal symmetry.

For a typical easy-plane antiferromagnet, $f^{\mathrm{mag}}_{\mathrm{in\ plane}}$ is much less than the effective constants (5) of magnetoelastic nature (see Table I). So in such a crystal destressing effects may stimulate the formation of domain structure and change the equilibrium orientation of the antiferromagnetic vector.

It should also be stressed that the three different shape-induced anisotropy constants (5) depend on the aspect ratio a/b in different ways. This opens the possibility of controlling macroscopic properties of the sample by varying its shape.

IV. FORMATION OF THE EQUILIBRIUM DOMAIN STRUCTURE

If the in-plane magnetic anisotropy is small but not vanishing, then the destressing energy favors formation of domain structure. For example, in the case of an isotropic sample ($a=b$) the only nontrivial term with $K_{\rm is}^{\rm elas}$ in Eq. (4) is nonnegative. In the absence of an external field it can only be diminished by zeroing the average values of $\langle L_x^2 - L_y^2 \rangle$ and $\langle L_x L_y \rangle$, i.e., by the appearance of equiprobable distribution of domains with different orientations of the antiferromagnetic vector.

The external magnetic field causes rotation of the antiferromagnetic vector and removes the degeneracy of various domains. Due to the long-range character of elastic forces, the field-induced ponderomotive force that acts on the domain wall is compensated by the destressing, restoring force. Competition of these two factors determines the equilibrium proportion of different domains. If, for example, the external field is applied parallel to an easy direction in the XY plane (say, the X axis), then the volume fraction ξ of energetically preferable Y-type domains (in which $\mathbf{L} \perp \mathbf{H}$) increases quadratically with field, $\xi = 0.5[1 + (H/H_{\rm MD})^2]$, up to the monodomainization field $H_{\rm MD} = \sqrt{K_{\rm is}^{\rm elas}/\chi} \propto \lambda'/\sqrt{\chi c_{44}}$.

The domain structure may also be observed in samples with small but nonzero eccentricity ($a \approx b$) providing that the in-plane magnetic anisotropy is large enough to keep two different equilibrium (stable and metastable) $\mathbf{L}$ orientations: $K_2^{\rm elas} \leqslant f_{\rm in\ plane}^{\rm mag}$. In this case it is the shape factor that removes the degeneracy and hence the equiprobability of the domains. In the above example, the fraction of X-type domains ($\mathbf{L} \| X$) depends on the aspect ratio as follows:

$$\xi - \frac{1}{2} = \frac{K_2^{\rm elas}}{K_{\rm 4an}^{\rm elas}} \propto \frac{b-a}{b+a}, \tag{7}$$

and the domain structure reproduces the orthorhombic symmetry of the sample.

The critical values of the aspect ratio $(a/b)_{\rm cr}$ (obtained from the condition $K_2^{\rm elas} = f_{\rm in\ plane}^{\rm mag}$) at which the equilibrium domain structure is still thermodynamically favorable are given in the last column of Table I.

V. TORQUE EFFECT

If the aspect ratio a/b of the sample noticeably differs from 1, then all the effective anisotropy constants in (4) have the same order of magnitude and are much greater than the in-plane anisotropy, $K_{\rm is}^{\rm elas} \gg f_{\rm in\ plane}^{\rm mag}$ (see Table I). So the sample has shape-induced uniaxial anisotropy regardless of its crystallographic symmetry.

An appropriate tool for measuring anisotropy constants is the rotational torque of an untwinned crystal in a magnetic field. If the rotational axis is perpendicular to the easy plane XY and the magnetic field makes an angle ψ with the X axis (see the inset in Fig. 1), then the rotational torque can be calculated as $-\partial\Phi/\partial\psi$, where the free energy potential Φ is given by Eq. (1). With account of Eqs. (4)–(6), the rotational torque per unit volume is represented as

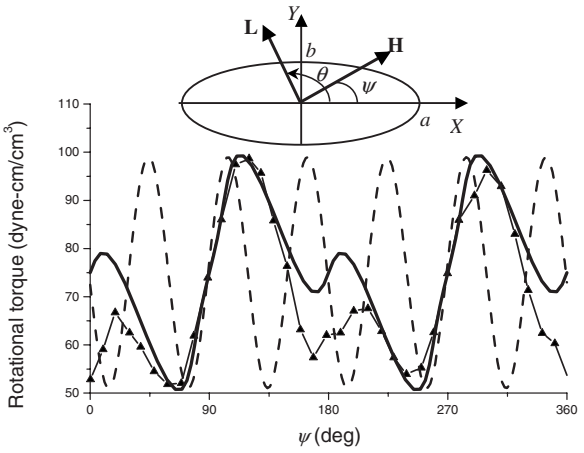

FIG. 1. Rotational torque of untwinned NiO crystal at room temperature (RT) in $H=4.8$ kOe for [111] rotational axis. Triangles, experimental data (Ref. 13); solid line, theoretical approximation according to Eqs. (8) and (9); dashed line, approximation of infinite crystal (no shape effect).

$$T(\psi) = K_2^{\rm elas} \sin 2\theta(\psi) + 2K_{\rm 4an}^{\rm elas} \sin 4\theta(\psi), \tag{8}$$

where θ is the angle between the antiferromagnetic vector and the X axis, which unambiguously determines the equilibrium orientation of $\mathbf{L}$ and is calculated from the condition for the minimum of the potential (1):

$$K_2^{\rm elas} \sin 2\theta + 2K_{\rm 4an}^{\rm elas} \sin 4\theta - \frac{1}{2}\chi H^2 \sin 2(\theta - \psi) = 0. \tag{9}$$

Analysis of Eqs. (8) and (9) shows that (i) the effective anisotropy is determined by shape-dependent (via the a/b ratio) constants $K_2^{\rm elas}$, $K_{\rm 4an}^{\rm elas}$; (ii) the shape-induced anisotropy removes the multiaxial degeneracy of equilibrium orientations of the antiferromagnetic vector and thus excludes formation of domain structure; (iii) in the absence of field the preferred orientation of the antiferromagnetic vector coincides with the longer ellipse axis ($K_2^{\rm elas} > 0$, $a > b$); (iv) an external magnetic field applied along the longer ellipse axis may induce a spin-flop transition at $H = H_{\rm SF}$, where the spin-flop field

$$H_{\rm SF} = \sqrt{\frac{1}{\chi}\left|K_2^{\rm elas} - 4K_{\rm 4an}^{\rm elas}\right|} \propto \frac{\lambda'}{\sqrt{\chi c_{44}}} \sqrt{\frac{a-b}{a+b}} \tag{10}$$

is governed by the sample shape and is independent of crystalline anisotropy.

An interesting result is obtained for a sample having a square cross section. In this case, the equilibrium distribution of the antiferromagnetic vector is in principle inhomogeneous but on average can still be described by Eq. (9) with

$$K_2^{\rm elas} = 0, \quad K_{\rm 4an}^{\rm elas} = \frac{\ln 2 (\lambda')^2}{\pi c_{44}(1-\nu)} > 0. \tag{11}$$

It is obvious that such a sample shows fourth-order effective anisotropy with easy axes directed along the square diagonals (45° angle with respect to the X axis, as results from the condition $K_{\rm 4an}^{\rm elas} > 0$).

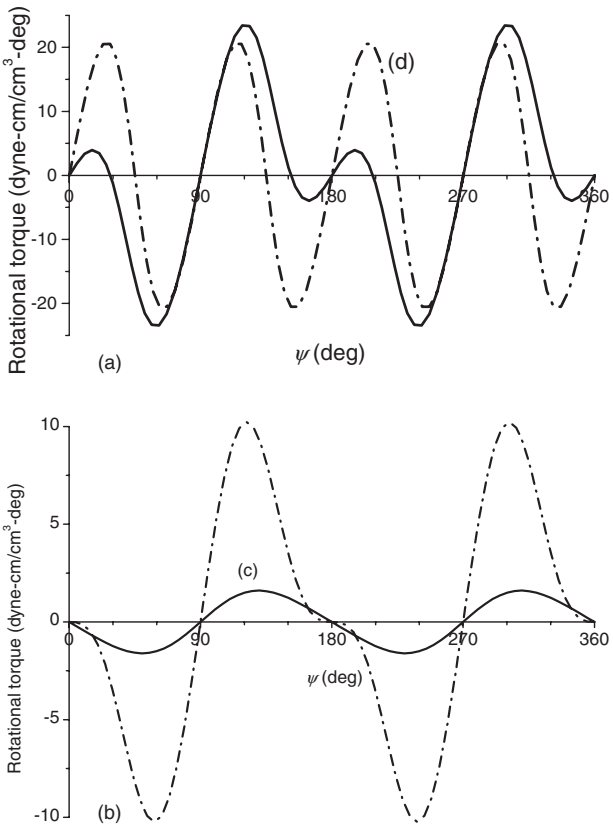

FIG. 2. Rotational torque (calculated) of untwinned NiO crystal at RT in $H=5$ kOe for [111] rotational axis for samples with different shapes. For ellipse-section samples the aspect ratio is $a/b=20$ (a), 3 (b), and 1.2 (c). (d) Square-section sample.

The rotational torque calculated from Eqs. (8) and (9) for a typical antiferromagnet NiO is shown in Figs. 1 and 2. In calculations we use the experimental results[13] for the rotational torque around the [111] axis taken at room temperature for $H=4.8$ kOe (triangles in Fig. 1). Since the experiment shows strong hysteresis in clockwise and counterclockwise rotations, the data in Fig. 1 are initially averaged over a clockwise-counterclockwise cycle. The theoretical curve (solid line) includes some nonzero average torque that may result from inhomogeneity of the sample, and the adjusted parameters are $\chi=4.35\times10^{-4}$ emu/cm^3, $K_2^{\text{elas}}=900$ erg/cm^3, $K_{4\text{an}}^{\text{elas}}=450$ erg/cm^3, $a/b=20$.

The four curves in Fig. 2 demonstrate possible variations of the rotational torque with the crystal shape. For a large aspect ratio (curve *a*), contributions from both second- and fourth-order anisotropy terms are equally important ($K_2^{\text{elas}} \propto K_{4\text{an}}^{\text{elas}}$); the torque curve is composed of $\sin 2\theta$ and $\sin 4\theta$ components. At lower aspect ratio (curves *b* and *c*), the fourth-order component becomes less pronounced and the amplitude of the torque also diminishes. A circular cylinder ($a=b$) will show no shape effect in a single-domain state, but a sample with a square cross section should possess fourth-order anisotropy (as seen from curve *d*), regardless of crystalline symmetry.

Evidently, shape dependence of the magnetic rotational torque for a NiO crystal was observed in Ref. 13. The authors notice that "a nearly pure $\sin 4\theta$ curve is obtained when the (111) cross section is square." For an arbitrary shaped section the experimental curve (Fig. 1, triangles) is satisfactorily fitted with a combination of $\sin 2\theta$ and $\sin 4\theta$ components (solid line). The dashed line in Fig. 1 shows the theoretical curve with $f_{\text{in plane}}^{\text{mag}}=220\cos 6\theta$ erg/cm^3, which could be expected in neglecting shape-induced effects. The presence of the $\sin 4\theta$ component in the rotational torque makes it possible to exclude the effect of **L** "freezing" by magnetoelastic strain, which may be expected in a relatively small magnetic field. Additional anisotropy induced by the frozen lattice is uniaxial and should be insensible to the variation of crystal shape.

VI. ANTIFERROMAGNETIC RESONANCE

The effect of shape-induced anisotropy may also be detected by measuring the frequency of the lowest branch of the spin-wave spectrum. The antiferromagnetic resonance (AFMR) frequency calculated within a standard Lagrangian technique in the long-wave approximation is given by the expression

$$\nu_{\text{AFMR}} = g\sqrt{\frac{2}{\chi}[K_{\text{is}}^{\text{elas}} + K_2^{\text{elas}}\cos 2\theta + 4K_{4\text{an}}^{\text{elas}}\cos 4\theta - \chi H^2\cos 2(\theta-\psi)]}, \tag{12}$$

where g is the gyromagnetic ratio and the equilibrium value of θ may be calculated from (9). The polar diagram of $\nu_{\text{AFMR}}(\psi)$ calculated from (12) for NiO ($g=2,5$) for a different crystal shape is shown in Fig. 3. For aspect ratio close to 1 (dotted line) the shape effect is negligible and the magnetoelastic gap in the AFMR spectrum is almost isotropic. For elongated (dash-dotted and dashed lines) or square-shaped (solid line) samples, the AFMR gap should show strong two- or four-fold anisotropy.

VII. SHAPE EFFECT IN ANTIFERROMAGNETIC NANOPILLARS

Taking into account recent interest in multilayered structures based on antiferromagnetic materials, we consider possible shape effects in the antiferromagnetic nanopillar that can be a constitutive part of spin-valve structure (see, e.g., Ref. 14). The typical nanopillar has the form of a very thin elliptic cylinder (thickness $c\approx 3-10$ nm) with a pronounced in-plane aspect ratio (with $a\propto 120$ nm and $b\propto 50$ nm).

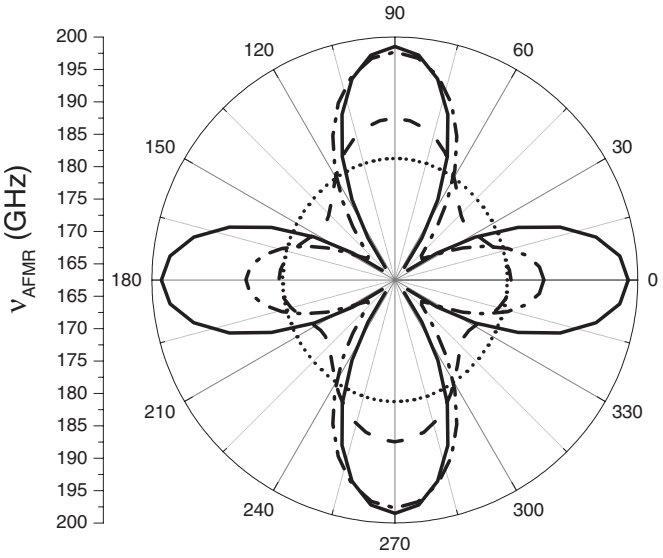

FIG. 3. Angular dependence of AFMR frequency vs magnetic field orientation for samples with different aspect ratio: $a/b=20$ (dash-dotted line), 3 (dashed line), and 1.2 (dotted line). Solid line corresponds to a square-section sample.

In this case ($c \ll a,b$) the constants of shape-induced anisotropy may be expressed through the parameter $k^2=1-b^2/a^2$ which depends on the aspect ratio $b/a \leqslant 1$, namely,

$$K_2^{\text{elas}} = \frac{c}{b}\frac{[(\lambda')^2(2-3\nu)+\lambda_v\lambda']J_2(k)}{4c_{44}(1-\nu)}, \quad K_{4\text{an}}^{\text{elas}} = \frac{c}{b}\frac{2(\lambda')^2 J_4(k)}{3c_{44}(1-\nu)}, \tag{13}$$

where we have introduced the dimensionless shape factors $J_{2,4}$ as follows:

$$J_2(k) = \int_0^{\pi/2} \frac{(\sin^2\phi + \cos 2\phi/k^2)d\phi}{\sqrt{1-k^2\sin^2\phi}},$$

$$J_4(k) = \int_0^{\pi/2} \frac{(1-8\cos 2\phi - k^2\sin^2\phi + 8\cos 2\phi/k^2)d\phi}{\sqrt{1-k^2\sin^2\phi}}. \tag{14}$$

Dependence of the shape factors $J_{2,4}$ vs aspect ratio calculated according to Eq. (14) is given in Fig. 4. It can be easily understood that both shape-induced constants (13) vanish for an isotropic sample ($b=a$). For all values of the aspect ratio the second-order term is greater than that of fourth order, $J_2 \geqslant J_4$. In the experimentally accessible range of values $b \propto 0.5a$ $J_2=0.52$ and $J_4=0.3$. Thus, the characteristic value of the shape-induced anisotropy in a stress-free thin film can be of the order of the magnetoelastic energy, $K_{\text{is}}^{\text{elas}} \propto (\lambda')^2/c_{44}$, multiplied by a small factor c/b that varies within the range 0.05–0.3 depending on the film thickness.

Substantial enhancement of the second-order shape-induced anisotropy K_2^{elas} should be expected in the case of mismatch between the antiferromagnet and substrate lattices. Lattice misfit is a source of rather strong (usually isotropic) in-plane stresses $\sigma_{xx}^{\text{mf}}=\sigma_{yy}^{\text{mf}}=\sigma^{\text{mf}}$ that should be added to the intrinsic stresses (3). The corresponding (and principal) contribution to the effective second-order anisotropy constant takes the form

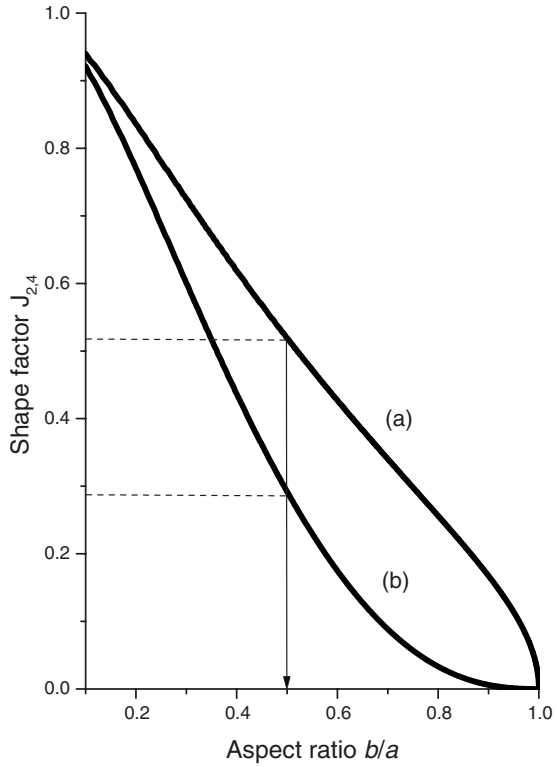

FIG. 4. Second- (a) and fourth-order (b) shape-induced anisotropy of a thin nanopillar as a function of aspect ratio. Arrow indicates the typical value of b/a used in the experiments (Ref. 14).

$$K_2^{\text{elas}} = \frac{c}{b}\frac{\sigma^{\text{mf}}\lambda' J_2(k)}{4c_{44}(1-\nu)}. \tag{15}$$

If u^{mf} is the lattice mismatch and $u^{\text{spon}} \propto \lambda'/c_{44}$ is an observable spontaneous strain that occurs at the Néel point, then we can estimate $\sigma^{\text{mf}} \propto c_{44}u^{\text{mf}}$ (with the assumption that the elastic moduli of substrate and antiferromagnet are of the same order of magnitude), $K_{\text{is}}^{\text{elas}} \propto (\lambda')^2/c_{44}$, and hence

$$K_2^{\text{elas}} \propto \frac{c}{b}\frac{u^{\text{mf}}}{u^{\text{spon}}}K_{\text{is}}^{\text{elas}}.$$

Substituting typical values of *small* lattice misfit $u^{\text{mf}}=0.005$ and *large* spontaneous striction $u^{\text{spon}}=10^{-4}$, we see that, even for very thin nanopillars with $c/b=0.05$, the shape-induced anisotropy may be as large as $K_2^{\text{elas}}=2.5K_{\text{is}}^{\text{elas}}$, and thus much greater than the bare in-plane magnetic anisotropy of antiferromagnet (see Table I).

The nontrivial relation (15) between the shape of the sample and the external stress produced by the substrate may reveal itself in switching of the shape-induced direction of the easy axis for different substrates. Really, if $K_2^{\text{elas}}>0$, then the equilibrium orientation of $\mathbf{L}$ in a monodomain sample is parallel to the ellipse's long axis a (X direction), as can be seen from (4) and the inset in Fig. 1. According to Eq. (15), the sign of K_2^{elas} depends upon the relation between intrinsic $(\lambda', u^{\text{spon}})$ and extrinsic $(\sigma^{\text{mf}}, u^{\text{mf}})$ stresses (or strains). In the

case when both substrate and eigen magnetoelastic forces of the antiferromagnet "work" in the same direction, trying to extend (compress) the crystal lattice, the product $\sigma^{mf}\lambda'$ will be positive (in accordance with the Le Chatelier principle) and $K_2^{elas}>0$. If we use another substrate which produces a misfit of opposite sign, $K_2^{elas}<0$, and the equilibrium orientation of **L** will be parallel to the short axis b (Y direction).

Control of spin orientation by substrate-induced strain was recently observed[15] in the antiferromagnet CoO. In bulk samples CoO is compressed in the **L** direction. When grown on a Mg(100) substrate, the CoO lattice is expanded in plane, and experiment shows that the Co spins go out of plane. And, in contrast, in-plane ordering is observed for a Ag(100) substrate, which produces a slight contraction in the film plane. From our point of view, analogous experiments with nanopillars would be very instructive in further study of shape-induced effect in antiferromagnetic crystals.

VIII. CONCLUSIONS

In summary, we propose a model that describes an antiferromagnet with pronounced magnetoelastic coupling. The model is based on the assumption that antiferromagnetic ordering is accompanied by the appearance of elastic dipoles. Due to the long-range nature of elastic forces, the energy of the dipole-dipole interaction (destressing energy) in a finite-size sample depends on the crystal shape and is proportional to its volume.

In easy-plane antiferromagnets with degenerate orientation of the easy axis, the destressing effects may stimulate formation of domain structure and redistribution of the domains in the presence of an external magnetic field.

The model predicts the existence of shape-induced magnetic anisotropy which corresponds to the macroscopic symmetry of the sample and can be detected by magnetic rotational torque and AFMR measurements.

The crystal shape may be a source of additional magnetic uniaxial anisotropy which produces different effects depending on the aspect ratio. Below some critical value of a/b, shape-induced anisotropy favors the formation of domain structure even in the absence of any external field. For large aspect ratio (above the critical value), shape-induced anisotropy removes the degeneracy of the easy axis in a single-domain sample. The energy difference between the easy and hard directions thus induced depends upon a/b. A square cross-section sample should acquire fourth-order anisotropy (irrespective of the crystal symmetry in the easy plane). This opens the possibility of controlling macroscopic properties of the sample by varying its shape.

The shape of antiferromagnetic nanopillars embedded into structures with lattice mismatch may be a principal source of magnetic anisotropy. This fact should be taken into account in engineering spin-valve devices.

[1] L. Néel, in *Proceedings of the International Conference on Theoretical Physics, Kyoto and Tokyo* (Science Council of Japan, Tokyo, 1953), p. 701.
[2] M. K. Wilkinson, J. W. Cable, E. O. Wollan, and W. C. Koehler, Phys. Rev. **113**, 497 (1959).
[3] B. K. Tanner, M. Safa, D. Midgley, and J. Bordas, J. Magn. Magn. Mater. **1**, 337 (1976).
[4] J. Baruchel, M. Schlenker, and W. L. Roth, J. Appl. Phys. **48**, 5 (1977).
[5] A. Janossy, F. Simon, T. Feher, A. Rockenbauer, L. Korecz, C. Chen, A. J. S. Chowdhury, and J. W. Hodby, Phys. Rev. B **59**, 1176 (1999).
[6] A. Scholl, J. Stöhr, J. Lüning, J. W. Seo, J. Fompeyrine, H. Siegwart, J. P. Locquet, F. Nolting, S. Anders, E. E. Fullerton, M. R. Schneifein, and H. A. Padmore, Science **287**, 1014 (2000).
[7] N. B. Weber, C. Bethke, and F. U. Hillebrecht, J. Magn. Magn. Mater. **226**, 1573 (2001).
[8] Y. Y. Li, Phys. Rev. **101**, 1450 (1956).
[9] V. M. Kalita, A. F. Losenko, S. M. Ryabchenko, P. A. Trotsenko, and T. M. Yatkevich, Fiz. Tverd. Tela (S.-Peterburg) **46**, 317 (2004).
[10] H. V. Gomonay and V. M. Loktev, Phys. Solid State **47**, 1755 (2005).
[11] M. Kléman and M. Schlenker, J. Appl. Phys. **43**, 3184 (1972).
[12] H. V. Gomonay and V. M. Loktev, J. Phys.: Condens. Matter **14**, 3959 (2002).
[13] W. L. Roth and G. A. Slack, J. Appl. Phys. **31**, S352 (1960).
[14] tjS. Urazhdin and N. Anthony, arXiv:cond-mat/0703281 (unpublished).
[15] S. I. Csiszar, M. W. Haverkort, Z. Hu, A. Tanaka, H. H. Hsieh, H.-J. Lin, C. T. Chen, T. Hibma, and L. H. Tjeng, Phys. Rev. Lett. **95**, 187205 (2005).